Journal of Inorganic and Organometallic Polymers and Materials (2019) 29:939–953
https://doi.org/10.1007/s10904-018-01069-w

Selective Photodegradation on Dual Dye System by Recoverable *Nano* SnO_2 Photocatalyst

D. Venkatesh[1] · S. Pavalamalar[1] · K. Anbalagan[1]

Received: 26 October 2018 / Accepted: 24 December 2018 / Published online: 21 January 2019
© Springer Science+Business Media, LLC, part of Springer Nature 2019

Abstract
A facile co-precipitation technique was developed to prepare SnO_2 nanoparticles using stannous chloride dihydrate ($SnCl_2{\cdot}2H_2O$) and characterized. The photocatalytic efficiency of *nano* SnO_2 was tested for degradation of Rhodamine B: $C_{28}H_{31}ClN_2O_3$ + (*nano* $SnO_2/\lambda = 254$ nm) + reactive species ($^{\bullet}O_2^{-}$, $^{\bullet}OH$, $^{\bullet}OOH$) $\rightarrow H_2O + CO_2$. In addition, mixture of Rhodamine B (RhB) and malachite green oxalate (MGO) were selected as the dual dye system (model pollutants) and their influencing factors such as concentration of mixtures (RhB + MGO), catalyst dosage, intensity of light source (254 and 365 nm), pH were also studied. Blank experiment (without catalyst) and surface adsorption indicates that Rhodamine B degrades at relatively very slow rate with $k = 2.30 \times 10^{-3}$ min^{-1} and $k = 2.4 \times 10^{-3}$ min^{-1} respectively. However, *nano* SnO_2 induces a large increment in degradation rate corresponding with $k = 4.0 \times 10^{-3}$ min^{-1} (RhB = 8.69×10^{-6} M, catalyst 50 mg/100 mL, $\lambda = 254$ nm) and mixed dyes $k_{RhB} = 18.96 \times 10^{-3}$ min^{-1} and $k_{MGO} = 26.5 \times 10^{-3}$ min^{-1} were obtained. Further, the reusability of the catalyst was sustained up to three cycles and verified with XRD pattern.

Keywords Nanoscale SnO_2 · Dual dye · Mixed pollutants · Photocatalysis

1 Introduction

Present day real-world wastewater from dye industries contains simple or mixture of organic dyes. Industries are releasing most notorious textile dyes, dye intermediates and inorganic contaminants into aquatic environment without appropriate disposal, this is very harmful to agriculture, human health and entire ecosystem due to their huge industrial production, slow biodegradation and toxicity. Dye molecules are very challenging to degrade by conventional techniques, due to their origin of synthetic routes aromatic structure and stability [1, 2]. Many synthetic dyes exhibit good resistance to irradiation sources (UV or solar light) and microbial treatment may produce more hazardous by-products during the degradation process [3]. Biodegradation techniques used to treat chemicals produce lot of toxic by-products with high concentration, which may cause carcinogenic, mutagenic and toxic effects to the living organism [4, 5]. Therefore, it is significant method to probe the photocatalytic activity of the catalyst both in simple and mixed dye solutions in order to decide the superior performance. Environmental friendly catalytic processes are increasingly receiving attention nowadays. Semiconducting nano materials are unique in nature because of their mechanical, optical, electrical, catalytic and magnetic properties. In semiconductors, the movement of electrons and holes are affected by size and geometry of the materials [6]. Recently, photocatalytic treatment of synthetic dye molecules has drawn considerable attention in waste-water treatment due to its low energy consumption and much less secondary pollution [7]. Among several semiconductors, nano scale tin oxide (SnO_2) is particularly pointed for its potential applications in microelectronics, gas sensing, protective coating, photovoltaic systems and photocatalysis [8]. Tin oxide (SnO_2) is an n-type semiconductor with a wide band gap ($E_g \geq 3.6$ eV) at room temperature with rutile-tetragonal phase structure and shows thermal and chemical stability, high reduction potential and high electron mobility for multiple applications in solar cells [9], gas sensors [10, 11], lithium-ion batteries [12, 13], and photocatalysts [14–17]. Catalytic properties of the SnO_2 nanoparticles are influenced by the grain size, morphology, large surface area, and generation of reactive species in the reaction [18].

✉ K. Anbalagan
kanuniv@gmail.com

[1] Department of Chemistry, Pondicherry University, Pondicherry 605014, India

Furthermore, the difference in valence band (VB) and conduction band (CB) edge potentials of SnO_2 nanoparticles leads to good electron–hole separation of photogenerated charge carriers, which enhances photocatalytic activity. Because of the high stability and low toxicity of insoluble SnO_2, the metal oxide can be utilized in the decomposition of environmentally harmful compounds and toxic wastes from water [19, 20]. Especially, Rhodamine B (RhB) has been proved to be a kind of dye pollutants, but widely used in leather, paper and textiles fields, might cause serious toxicities to public health [21]. Herein, a simple, low-cost, and scalable approach to construct SnO_2 nanomaterial is proposed. Mixed model pollutants such as, Rhodamine B (RhB) and malachite green oxalate (MGO) were taken as the toxic wastes to evaluate the photocatalytic activity of the sample.

2 Experimental Details

2.1 Materials and Methods

Rhodamine B and malachite green oxalate were purchased from Sigma-Aldrich and used as model compounds. *Nano* SnO_2 was prepared by a facile one-step co-precipitation approach with some modifications [22] using stannous chloride dihydrate ($SnCl_2{\cdot}2H_2O$). In a typical synthesis, 0.34 g of $SnCl_2{\cdot}2H_2O$ was dissolved in 1-propanol under constant magnetic stirring for 15 min and to this 0.18 g of dimethyl oxalate in 15 mL of deionized water was added slowly over a period of 10 min. The resulting mixture was agitated for approximately 10 min and the precipitate obtained was refluxed for a period of 24 h at ~ 85–90 °C. Then it was cooled to room temperature, centrifuged, washed several times with 1:1 de-ionized water and ethanol (v/v). Finally, the precipitate was dried in oven at ~ 110 °C for 10 h and subsequently annealed for 4 h at 500 °C.

2.2 Characterization

The phase identification of the nanomaterial was characterized by powder X-ray diffraction (XRD; Bruker,) with Cu Kα radiation (λ = 1.5405 Å). The optical absorption characteristics are determined with UV–Vis diffuse reflectance spectra by using a Shimadzu, UV 2450 double-beam spectrophotometer equipped with integrating sphere attachment (ISR-2200). The photoluminescence (PL) measurements were performed on a Spex FluoroLog-3 spectrofluorometer (Jobin-Yvon Inc.) using 450 W Xenon lamp and equipped with a Hamamatsu R928 photomultiplier tube. Photoluminescence and steady state decay were carried out and data fitting to exponential decay models was made using commercially available DAS6 v6.2 Horiba JobinYvon software packages. The goodness of fit was assessed by minimizing the reduced chi-squared function (χ^2). The size morphology and microstructure of the synthesized sample were examined by high-resolution transmission electron microscopy (HRTEM, JEOL 2010 at 200 kV), energy dispersive X-ray spectroscopy (EDS) was operated with an acceleration voltage of 200 kV.

2.3 Sorption Experiments

The surface adsorption experiments were carried out using Technico cooling water bath shaker at room temperature. *Nano* SnO_2 was added into 100 mL of aqueous solution of 8.69×10^{-6} mol/L (RhB) taken in a 125 mL stoppered glass bottle. Similarly, dual dyes, that is, RhB (8.69×10^{-6} mol/L, 50 mL) and MGO (1.08×10^{-5} mol/L, 50 mL) were mixed and used as model polluted water. The adsorption of dyes on the surface of catalyst at different time intervals; RhB = 0, 5, 10, 15, 30, 45, 60, 75, 90 and 105 min or RhB + MGO = 0, 15, 30, 60, 90 and 120 min were followed to estimate dye-surface affinity. The adsorbent was separated by centrifugation and the dye solution after adsorption was characterized spectrally.

2.4 Evaluation of Photocatalytic Activity

Degradation experiment was established by dispersing pure *nano* SnO_2 (50 mg) in aqueous RhB (8.69×10^{-6} mol/L, 100 mL), then the solution was magnetically stirred in dark for 60 min at room temperature to establish adsorption–desorption equilibrium between the catalyst and the dye. Similarly, in dual dye system, degradation was performed using *nano* SnO_2 (75 mg) in an aqueous mixture of 100 mL of RhB (8.69×10^{-6} mol/L, 50 mL) and MGO (1.08×10^{-5} mol/L, 50 mL). The experimental solution was then placed under UV light source (Heber Scientific, low pressure mercury vapor lamp, 6W, intensity measured; Light Meter, model: LX-1108, intensity of light of low pressure mercury lamp = 1800 lx) with maximum output at λ = 254 nm. The temperature was kept close to room temperature by water circulating pump. Three milliliter aliquots from the photochemical reactor (quartz tube, capacity 100 mL, dia of inner-outer jacket = 0.5 cm) were drawn at definite time intervals (RhB = 0, 5, 10, 15, 30, 45, 60, 75, 90, and 105 min and dual dye system, RhB + MGO = 0, 15, 30, 60, 90 and 120 min), centrifuged and spectrally analyzed [λ_{max} ~ 554 (RhB) and λ_{max} ~ 616 (MGO)] to determine the concentration of dye.

The degradation efficiency was estimated using the relationship: $[C_0 - C/C_0]\times100$, where C_0 is the initial concentration and C at various time intervals. Control experiments were carried out parallel to confirm the photocatalytic degradation of dye molecules during the reaction. Further investigation on the photodegradation was made in presence of scavengers. To do this, a number of compounds like,

2-propanol (Pr^iOH) was added as the hydroxyl ($^\bullet OH$) radical scavenger, p-benzoquinone as the superoxide ($^\bullet O_2^-$) scavenger, EDTA-2Na as the hole (h^+) scavenger, sodium azide as the singlet oxygen ($^1O_2$) scavenger for RhB and dual dyes.

2.5 Electrochemical Measurements

Cyclic voltammograms were obtained using AUTOLAB interface electrochemical analyzer consisting of three electrode configurations such as; platinum auxiliary electrode (0.3 mm diameter), Ag/AgCl-sat. KCl reference electrode and the working electrode was prepared by mixing *nano* SnO_2 active material, carbon black and poly (vinylidene fluoride) as a binder in a weight ratio of 70:20:10 and slurry was made using *N*-methyl-2-pyrrolidone. The slurry was coated on a stainless steel (5 µm thickness) and dried at 80 °C under vacuum. A glass cell vial with fitted-top can accommodate three electrodes and a gas purging tube, then supporting electrolyte solution was deoxygenated by purging with nitrogen gas for 10–15 min. Pt electrode surface was polished with 0.05 µm gamma alumina powder, afterwards rinsed thoroughly with de-ionized water and acetone to ensure homogeneity. The cyclic voltammetric studies were carried out in 0.1 M sulphuric acid as a supporting electrolyte at various scan rates 50–250 mV/s in the potential range of − 0.3 to 0.8 V using Autolab workstation.

3 Results and Discussion

Tin oxide nanoparticles were obtained through an altered approach in a one-step co-precipitation technique using dimethyl oxalate as the precipitator. The nanoscale particles were characterized and the photocatalytic activities (light source; 365, 254 nm) were tested with Rhodamine B model dye. The efficiency of the catalyst was also examined for a dual dye system consisting of a mixed solution of Rhodamine B and malachite green oxalate.

3.1 XRD Analysis

The crystallographic structure and phase purity of the sample was confirmed by PXRD analysis. Crystal phase identification was undertaken for the freshly prepared and recovered *nano* SnO_2 catalyst. Figure 1 supplies the X-ray diffraction (XRD) patterns of the freshly prepared SnO_2 and catalyst recovered from photolyte solution after dye degradation process. The diffraction pattern of the fresh *nano* SnO_2 is in close resemblance with the pattern of recovered *nano* SnO_2. All of the diffraction peaks for these samples could be well indexed as the tetragonal rutile phase (JCPDS File no. 41-1445). The peak positions $2\theta = 26.611$, 33.893, 37.949, 51.780, 54.757, 57.818, 61.870, 64.717, 71.276 correspond

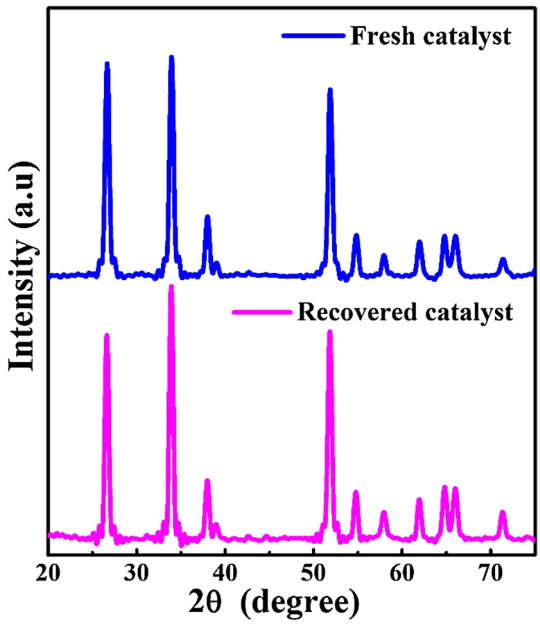

Fig. 1 X-ray diffraction pattern of *nano* SnO_2 obtained from co-precipitation technique and recovered catalyst after photolysis of Rhodamine B at room temperature

to the (110), (101), (200), (211), (220), (002), (310), (112), (202) lattice planes of tetragonal rutile SnO_2 [23]. The peaks are very sharp, intense showing high degree of crystallinity of the samples. It means crystalline nature was retained even after photolysis and no impurities were ascribable and detectable. The average crystallite size was calculated to be 15.68 nm (Debye–Scherrer equation) for the fresh and recovered (19.72 nm) samples.

3.2 Optical Property

Nano SnO_2 was studied by UV–Vis diffuse reflectance spectroscopy (DRS). Spectrum was acquired mainly here to determine the respective band gap value. Figure 2a depicts DRS curve for the nanoparticles, presenting reflection maximum in which a strong absorption edge at ca. 490 nm appears. This can be ascribed to the larger energy band gap of rutile phase of SnO_2, moreover, a strong absorption in the ultraviolet region is due to the electronic interaction of metallic center to the influence of charge delocalization [24]. The optical band gap of *nano* SnO_2 was elucidated using the relationship: $[F(R)h\nu]^n = A\,(h\nu - E_g)$ in which hν, A and E_g are the incident photon energy, proportional constant, and optical band gap, respectively and optical absorption coefficient using Kubelka–Munk function. The exponent 'n' equals 2 (direct transition) or 1/2 (indirect transition) and extrapolating the linear portion of the plot of $[F(R)h\nu]^2$ versus $h\nu$, the optical band gap (E_g) could be determined (inset Fig. 2a). Here, the direct band gap energy of the sample

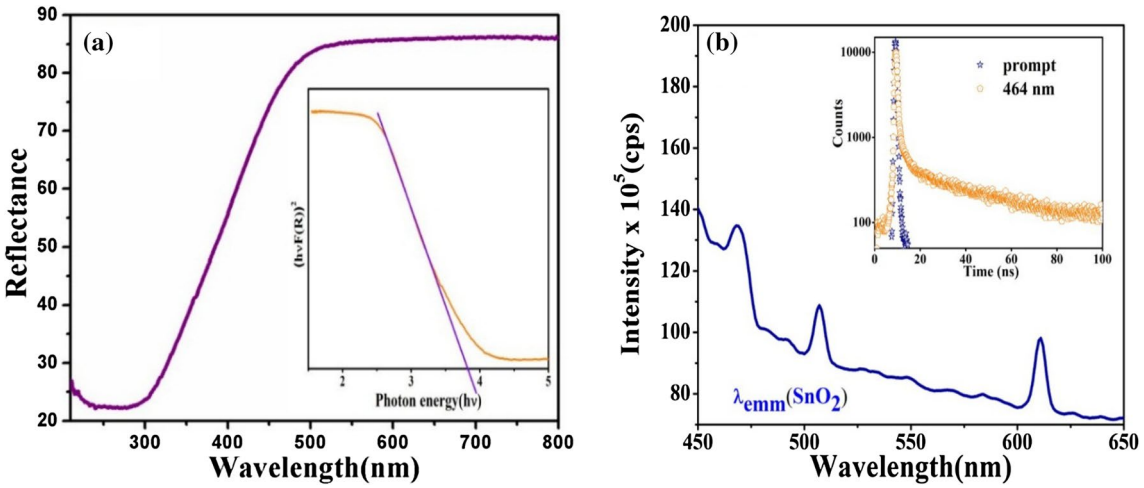

Fig. 2 **a** Kubelka–Munk transformation of diffuse reflectance spectrum of *nano* SnO_2. (Inset **a**) The band gap energy can be estimated by extrapolation of $[F(R)h\nu]^2$ versus $h\nu$. **b** Steady state exciton emission spectrum of *nano* SnO_2. (Inset **b**) Time resolved luminescence profile observed at $\lambda_{exc} = 464$ nm (orange curve). Steady-state PL, a prompt is shown for comparison (solid royal blue line). (Color figure online)

was estimated to be 3.8 eV. The larger band gap obtained may also be due to the formation of rutile phase of SnO_2, annealed at high temperature.

Photoluminescence (PL) spectroscopy is an important technique to study the luminescent behavior of sample and its results deliver recombination of free charge carriers in a semiconductor. PL spectrum can be useful to understand the effective separation and recombination process of photogenerated electrons (e^-) and holes (h^+) on the sample surface [25]. Photoluminescence spectra of the *nano* SnO_2 particles under wavelength of excitation at 370 nm were measured (in Fig. 2b) and the observed peaks were at 468, 507 and 611 nm. In nanoscale dimensions, the efficiency of emission exciton is inhibited due to the same 'even parity' of the conduction (CB) and valence (VB) bands. Generally, the visible range signals at 468, 507 and 611 nm wavelength originates from the surface defects, such as tin interstitial, dangling bonds, or oxygen vacancies in the samples [26]. Figure 2b (inset) illustrates time-decay curve of the *nano* SnO_2 particles with an emission at 464 nm fits well to a triexponential function $[I = \Sigma_n A_n \exp(-t/\tau_n)]$, where A_n and τ_n represent the amplitude and lifetime of the components, respectively, containing a fast part with a characteristic time of ~ 30 ps and a slow part with a characteristic time of 300–400 ps. Table 1 presents data for the decay process of tin oxide nanoparticles (464 nm): 19.08 ns (τ_1), 285.38 ns (τ_2) and 1.84 ns (τ_3) respectively.

3.3 TEM and EDX Profile

Figure 3a–d show transmission electron microscopy (TEM) images, as well as the selected area electron diffraction (SAED) patterns, inverse fast Fourier transform (IFFT) and EDX profile to confirm the size and morphology of SnO_2 nanoparticles. The size of the SnO_2 is in the range 16–24 nm and similar particle size was also observed from XRD pattern. Figure 3a reveals TEM micrographs of tin oxide nanoparticles that are spherical in shape with even size particle distribution and slightly agglomerated corresponding to tetragonal rutile tin oxide structure. The SAED pattern is well-dispersed in the case of tin oxide nanoparticles and suggest good crystalline structure, lattice planes and d-spacings (110), (101), (211) and (301) which match well (JCPDS 41-1445) with the rutile phase of SnO_2 [27].

Table 1 UV–Vis diffuse absorption, band gap energy, photoluminescence spectra and decay data of *nano* SnO_2 at room temperature

Sample name	DRS spectrum		Photoluminescence spectrum		Life time (ns)				
	Absorption edge (nm)	Band gap energy (eV)	λ_{emi} (nm)	Intensity $\times 10^5$ cps	λ_{emi} (nm)	τ_1	τ_2	τ_3	χ^2
SnO_2 NPs	370	3.8	468	136	464	19.08	285.38	1.84	1.16
			507	108					
			611	98					

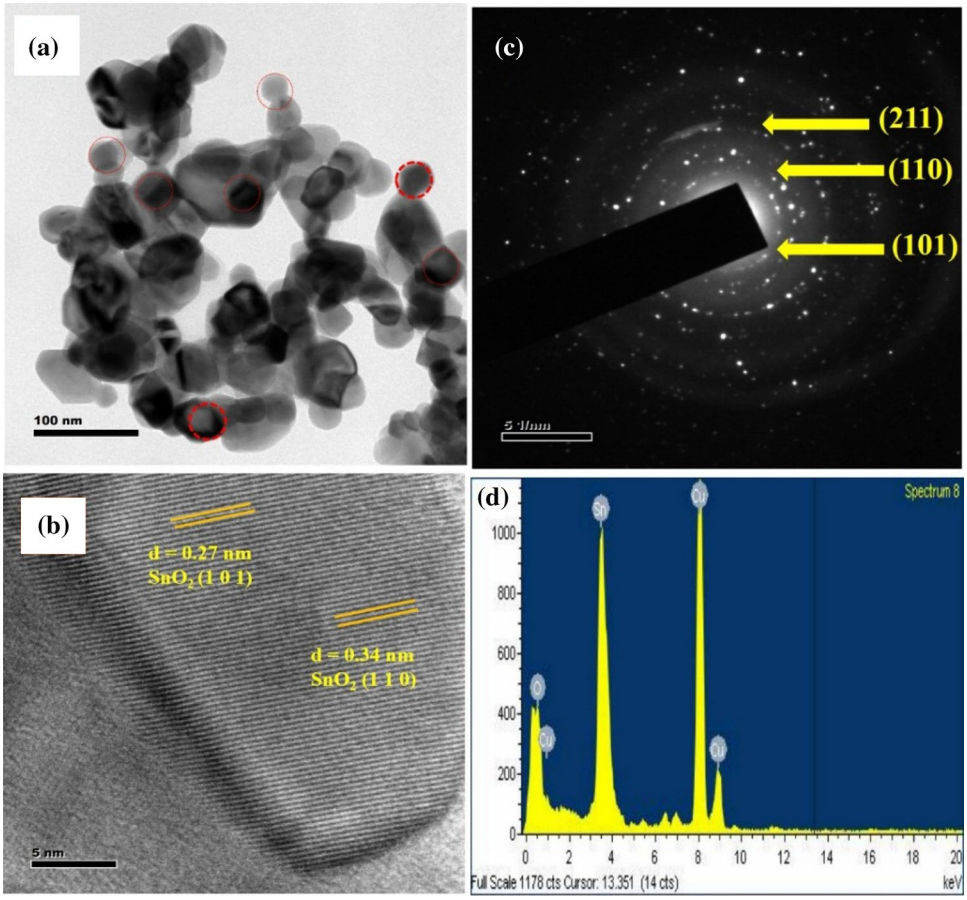

Fig. 3 **a** TEM magnification (100 nm) micrographs of *nano* SnO_2, **b** inverse fast Fourier transform with indexing for relevant lattice spacing, **c** SAED pattern of sample, **d** EDX profile. The TEM profile was recorded using copper grid

Figure 3b shows the various inter planar distances such as 0.34 and 0.27 nm correspond to the SnO_2 (110) and (101) low-index facets. In addition, EDX profile confirms the Sn and O elements in the sample and absence of any other impurities in the sample.

3.4 Electrochemical Measurement

The cyclic voltammetry curves of SnO_2 nanoparticles were obtained at the scan rate 50–250 mV s^{-1} in the potential window of −0.3 to 0.8 V (0.1 M H_2SO_4). Figure 4 exhibits ideal rectangular shape cyclic voltammograms representing electric double-layer capacitance of the sample. Further, the curves are symmetrical at varied scan rate of measurement suggests good electrochemical capacitive characteristics. Moreover, the active materials show low resistance and fast electronic transport rate upon increasing the scan rate [28]. It is clear that the materials possess recyclable stability and good pseudocapacitive behavior. This contributes electrochemical charge storage leading to a system for higher capacitance.

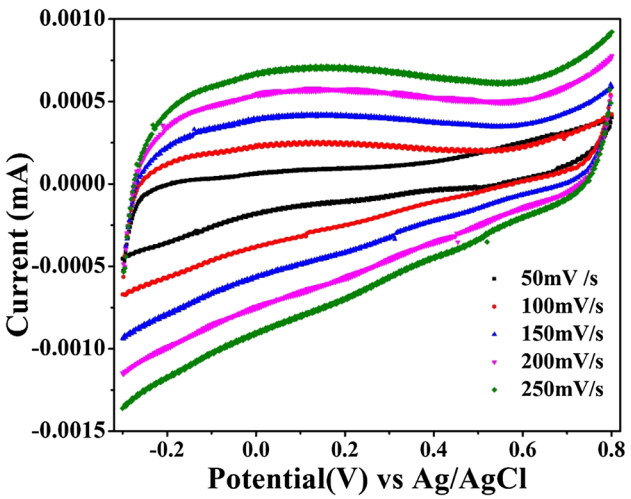

Fig. 4 Cyclic voltammogram of *nano* SnO_2 using 0.1 M H_2SO_4 as a supporting electrolyte; platinum as an auxiliary electrode, Ag/AgCl as a reference electrode, working electrode prepared by weight ratio of active material, carbon black and poly (vinylidene fluoride) (70:20:10) slurry with *N*-methyl-2-pyrrolidone

3.5 Surface Sorption and Photodegradation

Generally, the catalysis behavior is very much dependent upon the surface morphology, oxygen defects, particle size, surface-to-volume ratio, crystallinity and species involved in the reaction [29]. Surface adsorption characteristics of dye molecules also imply significance in the catalytic efficiency of a photocatalyst. A preliminary experiment of sorption and desorption was conducted to determine a comparison of the timescale of degradation reaction of dye with that of sorption and desorption of RhB on *nano* SnO_2. Here, negative surface charge of SnO_2 electrostatically attract the cationic dye molecules such as Rhodamine B and malachite green oxalate, which can facilitate the degradation process [30]. From the sorption studies the adsorption–desorption process was achieved within time scale that can enhance the catalytic activity. In general, the adsorption process of RhB dye molecules on the nanoparticles closely approaches equilibrium within ~ 60 min. However, no significant changes are observed after 60 min upto a maximum of ~ 105 min, however, within this timescale about 17% and 21% of RhB dye was adsorbed on the catalyst (50 mg/100 mL). The desorption experiment illustrates the re-equilibration was almost completed within 60 min in SnO_2. In the case of dual dye system: Rhodamine B = *ca.* 5% (60 min) and 7% (120 min) and malachite green oxalate = *ca.* 32% (60 min) and 37% (120 min) were loaded on the catalyst at *ca.* 75 mg in 100 mL as presented in Fig. 5a, b.

Photocatalytic reduction of RhB and mixed dyes were tested using *nano* SnO_2 in solution and the track of time-dependent degradation curves are presented in Fig. 6a, b and the degradation efficiency of RhB and mixed dyes (RhB + MGO) are presented in Tables 2, 3 and 4. The progression of the degradation was monitored from the disappearance of color at the characteristic absorption maxima: λ_{max} ~ 554 nm (RhB) and λ_{max} ~ 616 nm (MGO) in dual dye system (Inset Fig. 6a, b). Some opposite experiments on dual dye system with no light and without catalyst were also conducted, however, the efficiency was low. A very weak performance of dye degradation in former case was observed, but an enhanced performance for the latter was noted with time gone. The rate constants were obtained using Langmuir Hinshelwood model, which relates the reaction rate to the concentration of the organic pollutant as: [31] $r = -dc/dt = k_r K_{ad} C/(1 + K_{ad} + C)$, where r is the reaction rate, C is the concentration of the pollutant, t is the reaction time, k_r is the intrinsic rate constant and K_{ad} is the adsorption equilibrium constant. When the concentration of the pollutant is very low, equation can be simplified to $\ln (C_0/C)\ k_r K_{ad} t = kt$, where k is the apparent first order rate constant. Therefore, linear plot of $\ln C_0/C$ versus t are generally applicable and the data are provided in Tables 2, 3 and 4. The blank experiment (without catalyst) and surface adsorption indicates that Rhodamine B degrades at relatively very slow rate with $k = 2.30 \times 10^{-3}$ min^{-1} and $k = 2.4 \times 10^{-3}$ min^{-1} respectively. However, *nano* SnO_2 induces a large increment in degradation rate corresponding with $k = 4.0 \times 10^{-3}$ min^{-1} (RhB = 8.69×10^{-6} M, catalyst 50 mg/100 mL, $\lambda = 254$ nm) and mixed dyes $k_{RhB} = 18.96 \times 10^{-3}$ min^{-1} and $k_{MGO} = 26.5 \times 10^{-3}$ min^{-1} were obtained.

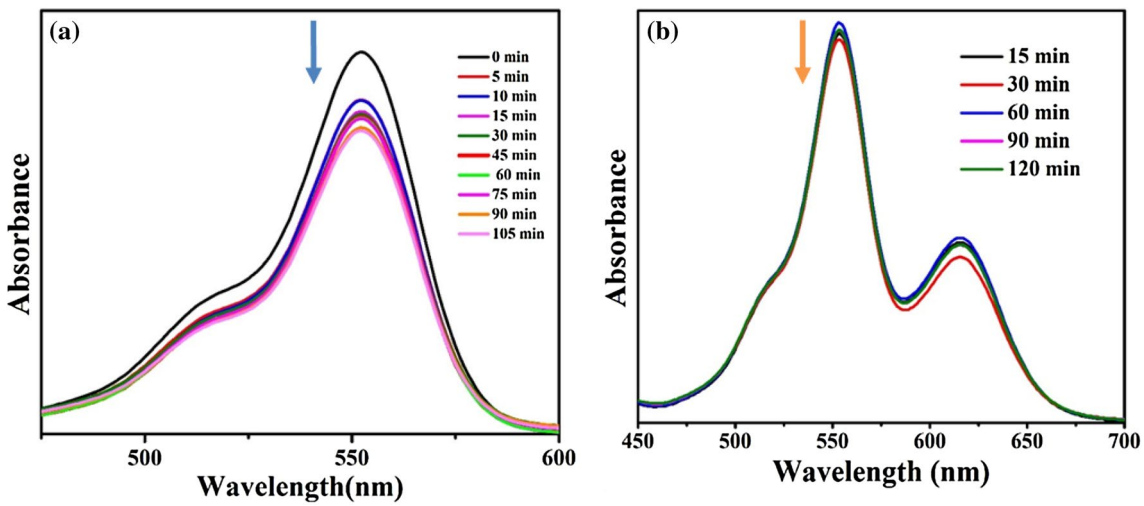

Fig. 5 **a** Time dependent UV–Vis absorption spectra of Rhodamine B (catalyst = 50 mg /100 mL). **b** Mixture of malachite green oxalate and Rhodamine B solution (catalyst = 75 mg/ 100 mL) by sorption experiments at room temperature

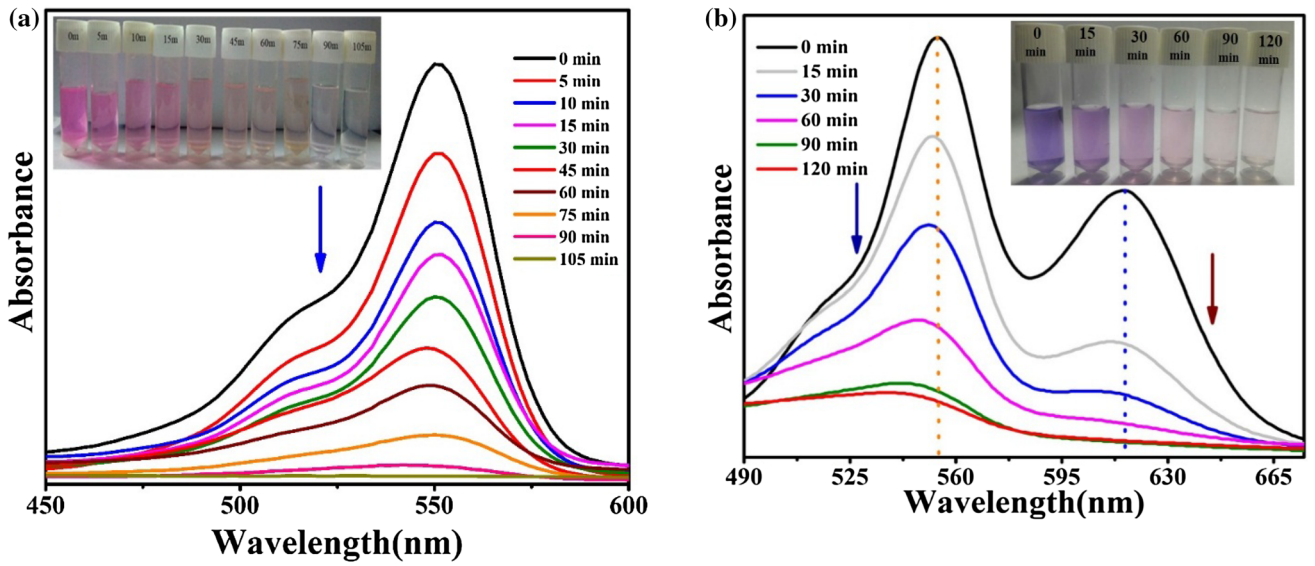

Fig. 6 Time dependent UV–Vis absorption spectra of degradation of Rhodamine B and mixed dye of malachite green oxalate and Rhodamine B under ultra violet light irradiation (λ ~ 254 nm) catalyzed by *nano* SnO_2 at room temperature

4 Role of Factors in Photocatalysis

Various photocatalytic experiments were carried out to control the reaction condition such as concentration of RhB and mixed dye molecules, quantity of the catalyst, pH, and intensity of the light sources. In the first study, the concentration of dye was varied (Rhodamine B, 8.69×10^{-6} to 1.04×10^{-5} mol/L, RhB: catalyst 50 mg/100 mL, RhB + MGO: catalyst 75 mg/100 mL) and it was found that the dye is degrading efficiently at low concentration. This may be due to the more available surface sites for exposure to light as number of molecular adsorption is less, also production of intermediates and carbonaceous deposits on the catalyst during dye degradation is less. These would lead to the enhanced number of photons available to reach the photocatalyst surface and improved number of oxidative species, thus causing pronounced dye degradation [32]. Figures 7a, 8a and 9a confirm that at lower concentration more degradation rate was observed and higher concentration of pollutants reduces the intensity of light source to reach the surface of the catalyst, degradation rate was also decreased. In the second study, photocatalyst dosage enhancement allows more number of adsorption sites and provides more active sites for oxidative species formation ($^{\bullet}O_2^-$, and $^{\bullet}OH$) leading to a significant enhancement of the adsorbed dye molecules degradation rate [33]. The quantity of nano scale tin oxide was optimized by varying photocatalyst in the range 30–50 mg/100 mL for RhB solutions and 50–100 mg/100 mL for mixed dye solutions. Figures 7b, 8b and 9b depict 50 mg in 100 mL dosage (Rhodamine B 99%) and 75 mg in 100 mL (RhB + MGO) high yields on the degradation rate was observed. The optimized catalyst density produce more number of photons are probably entering through much diluted dye solution so as to effectively reaching the surface of catalyst and promote electron/hole generation [34]. In the third study, the intensity of light source (254 nm) at constant catalyst 50 mg *nano* SnO_2 in 100 mL, for RhB degradation, 75 mg nano SnO_2 in 100 mL for mixed dye (MGO + RhB) and the results were also obtained by varying medium of the pH solution. The pH of an aqueous medium can influence the photocatalytic process through absorption between dyes and the catalyst surface and redox processes of photocatalysts [16]. Figures 7c, 8c and 9c reveal that the maximum degradation rate is achieved at pH 7 (99%) for RhB and mixed dye molecules (pH 7 for RhB and pH 9 for MGO). The optimum degradation rate of RhB and mixed dye (RhB + MGO) was observed at neutral medium, while pH range 4 and 9 permit decreased catalytic activity. In an acidic medium the surface charge and dispersion of nanoparticles are affected. Secondly, the catalyst surface charge is negative which results in increasing stronger electrostatic repulsion with dye molecules. It means that negatively charged catalyst prevented adsorption of hydroxide ions, diminishing oxidative species in the reaction [35]. In alkaline medium, the interaction between the organic pollutant and generation of reactive species, dissolved oxygen are more on the surface of the catalyst to enhance the photocatalytic activity.

Figures 7d, 8d and 9d show that the degradation of RhB and mixed dyes were performed under 254 and 365 nm

Table 2 Time dependent photodegradation efficiency and *rate constant* data for the degradation of Rhodamine B on *nano* SnO_2 by varying parameters at room temperature

Reaction conditions	Time (min)									Rate constant (RhB)	
	5	10	15	30	45	60	75	90	105		
	Degradation efficiency of RhB (%)									$\times 10^{-3}$ (min)	r^2
No catalyst	46	47	49	50	51	54	55	56	56	2.3	0.83
No light	17	18	20	25	27	31	34	35	36	3.5	0.82
Surface adsorption	13	13	16	16	17	17	18	20	21	2.4	0.68
Effect of concentration											
8.69×10^{-6} M	14	21	38	56	68	76	88	96	99	4.0	0.92
9.39×10^{-6} M	22	34	41	47	68	70	84	86	88	2.1	0.97
1.04×10^{-5} M	31	33	35	42	52	62	68	72	77	1.3	0.96
Effect of dosage											
30 mg/100 mL	31	51	52	56	68	73	82	85	93	2.8	0.99
40 mg/100 mL	55	59	63	70	80	86	89	90	94	2.9	0.97
50 mg/100 mL	14	21	38	56	68	76	88	96	99	4.0	0.92
Effect of pH											
pH 4	34	58	84	85	91	91	91	96	97	3.3	0.85
pH 7	14	21	38	56	68	76	88	96	99	4.0	0.92
pH 9	18	29	34	58	68	80	87	89	92	2.5	0.99
Intensity of light source											
254 nm	14	21	38	56	68	76	88	96	99	4.0	0.92
365 nm	6	11	12	14	15	18	26	30	30	3.3	0.93

Data calculation: efficiency in terms of ±01; rate constant ± 0.01

Table 3 Time dependent photodegradation efficiency and *rate constant* data of Rhodamine B from the mixture (RhB + MGO) on *nano* SnO_2 by varying parameters at room temperature

Reaction conditions (RhB ~ 554) from the mixture	Time (min)					Rate constant (RhB)	
	15	30	60	90	120		
	Degradation efficiency (%)					$\times 10^{-3}$ (min)	r^2
No catalyst	6	10	16	23	23	2.5	0.94
No light surface adsorption	17	17	17	17	19	1.7	0.25
Effect of concentration[a]	3	5	5	6	7	0.6	0.76
4.35×10^{-6} M	23	45	68	84	86	18.96	0.97
8.69×10^{-6} M	10	16	28	41	49	5.7	0.99
8.69×10^{-6} M	12	13	20	29	39	4.1	0.96
Effect of dosage							
50 mg/100 mL	10	19	35	50	56	7.5	0.99
75 mg/100 mL	23	45	68	84	86	18.96	0.97
100 mg/100 mL	14	15	15	26	28	2.8	0.82
Effect of pH							
pH 4	19	19	36	40	44	4.7	0.89
pH 7	23	45	68	84	86	18.96	0.97
pH 9	41	54	59	74	79	13.27	0.90
Intensity of light source							
254 nm	23	45	68	84	86	18.96	0.97
365 nm	31	31	39	42	44	5.04	0.64

[a]Concentration of Rhodamine B from the mixture (RhB + MGO); data calculation: efficiency in terms of ± 01; rate constant ± 0.01

Table 4 Time dependent photodegradation efficiency and *rate constant* data of malachite green oxalate from the mixture (RhB + MGO) on *nano* SnO_2 by varying parameters at room temperature

Reaction conditions (MGO ~ 616) From the mixtures	Time (min)					Rate constant (MGO)	
	15	30	60	90	120		
	Degradation efficiency (%)					$\times 10^{-3}$ (min)	r^2
No catalyst	38	42	49	57	69	9.4	0.87
No light	38	52	53	56	57	7.7	0.52
Surface Adsorption	30	31	32	32	37	3.8	0.37
Effect of concentration[a]							
5.40×10^{-6} M	57	77	87	94	94	26.7	0.89
1.08×10^{-5} M	19	33	58	74	82	14.8	0.99
2.14×10^{-5} M	16	17	33	48	64	8.6	0.97
Effect of dosage							
50 mg/100 mL	42	55	71	82	86	17.3	0.95
75 mg/100 mL	57	77	87	94	94	26.75	0.89
100 mg/100 mL	33	39	46	61	70	9.9	0.93
Effect of pH							
pH 4	55	55	75	84	85	17.5	0.88
pH 7	57	77	87	94	94	26.75	0.89
pH 9	94	98	99	99	99	40.1	0.49
Intensity of light source							
254 nm	57	77	87	94	94	26.75	0.89
365 nm	69	81	81	85	86	17.5	0.53

[a]Concentration of malachite green oxalate from the mixture (RhB + MGO); data calculation: efficiency in terms of ± 01; rate constant ± 0.01

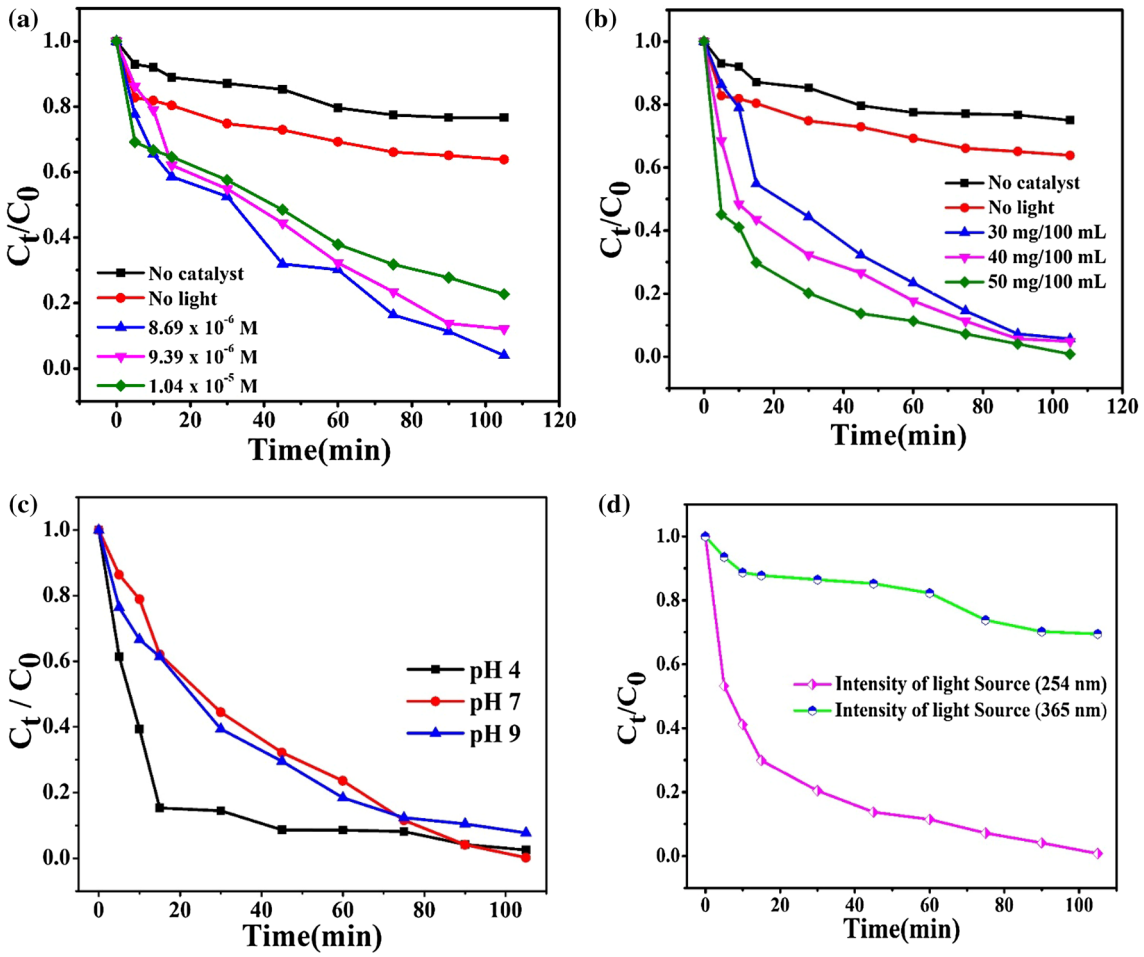

Fig. 7 Factors influencing photocatalytic degradation of Rhodamine B. Effect of **a** concentration, **b** catalyst dosage, **c** pH, **d** intensity of light source (254 and 365 nm)

irradiation. It was observed that, degradation of RhB and mixed dyes (RhB + MGO) increased with 254 nm > 365 nm at given intensity of light source. In higher wavelength, the inability to promote more electrons-holes combination and oxidative species during the photocatalytic reactions to degrade the RhB and mixed dyes. This indicates that, more electrons and holes are produced per unit time and efficient reactive radical formation to degrade the dye molecules at faster rate at lower wavelength [36].

4.1 Effect of Radical Scavenger

Participation of reactive species, scavengers experiments were examined to elucidate the possible pathway or mechanism involved in the photocatalytic reaction. Photoexcitation of *nano* SnO_2 leads to agglomeration of holes in the valence band: h^+ (SnO_2 VB) and migration of electrons into the conduction band: e^- (SnO_2 CB). Subsequently, h^+ (SnO_2 VB) are trapped by surface-linked hydroxyl groups, generating $^{\bullet}OH$, a powerful oxidizing agent, this can decompose organic dyes. The e^- (SnO_2 CB) reduces oxygen molecule and produce superoxide anion radical, $^{\bullet-}O_2$, and $^{\bullet}OOH$ radical. To probe different reactive species during the photocatalytic degradation of RhB and mixed dyes (RhB + MGO) neat, N_2-bubbled, and different scavenger influenced conditions were carried out. In brief, Fig. 10a confirms that the efficiency of degradation is minimized from RhB; 99% (no scavenger) → 30% (N_2-bubbled). This is in conformity with participation of O_2, which can serve as an efficient electron scavenger. Additional experiments were carried out with scavengers such as, isopropanol (60 µL mol L^{-1}) as the hydroxyl ($^{\bullet}OH$) radical scavenger, and p-benzoquinone (0.108 g mol L^{-1}) as the superoxide ($^{\bullet}O_2^-$) scavenger, EDTA-2Na (0.166 g mol L^{-1}) as the hole (h^+) scavenger and sodium azide (0.065 g mol L^{-1})as the singlet oxygen ($^1O_2$) respectively [37, 38]. The result shows that only a very slight degradation can be achieved when O_2 is excluded by N_2-purging. Figure 10a reveal that the photodegradation efficiency of Rhodamine B decreased

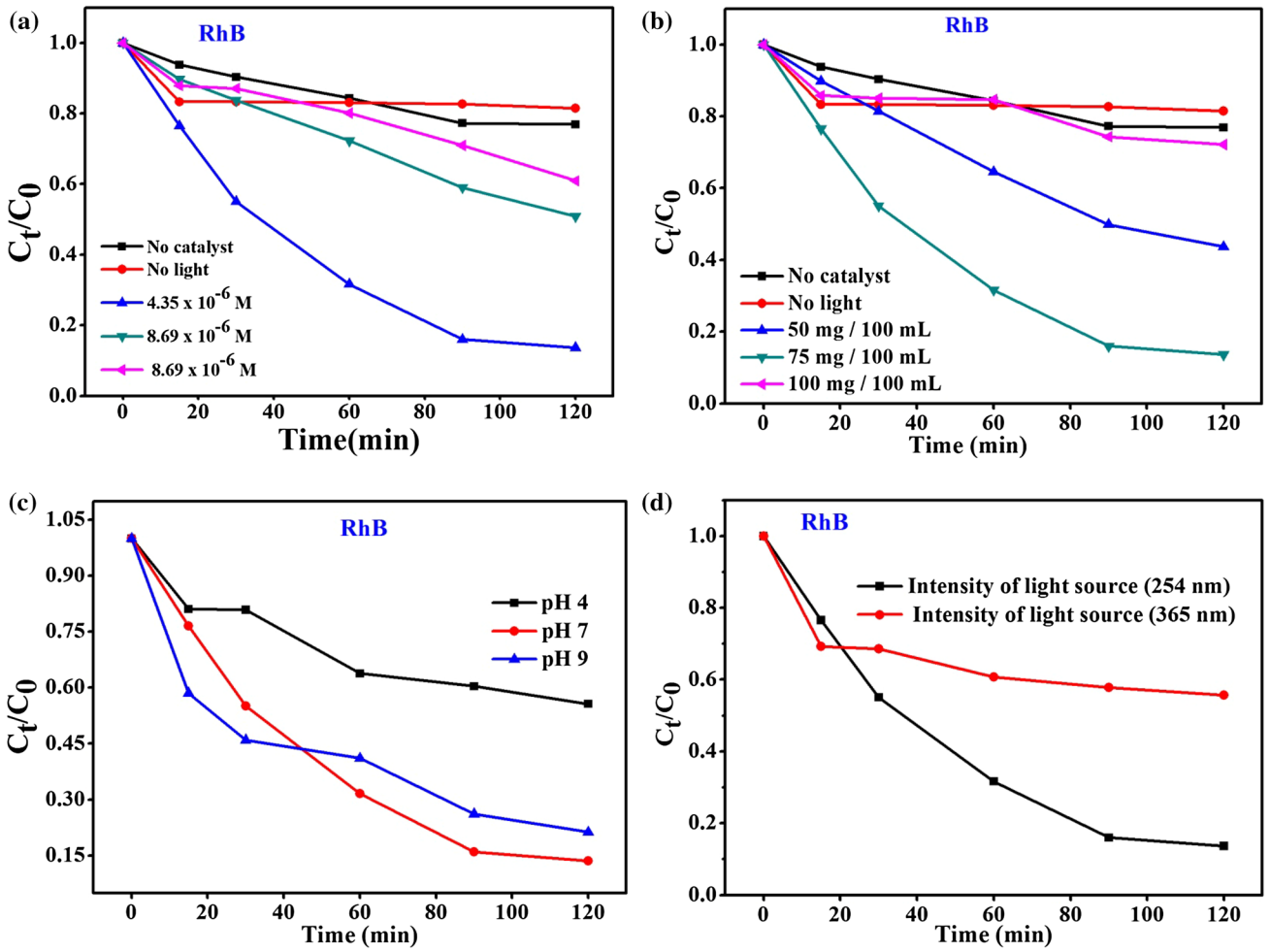

Fig. 8 Factors influencing photocatalytic degradation of Rhodamine B (λ ~ 554) from the mixtures. Effect of **a** concentration of Rhodamine B from the mixtures (RhB + MGO), **b** catalyst dosage, **c** pH, **d** intensity of light source (254 and 365 nm)

from 99% into 24%, 53%, 47%, 70% after addition of isopropanol, p-benzoquinone, EDTA-2Na and sodium azide scavengers, respectively. This result shows that both charge carriers and reactive radicals are responsible by the same extent for photocatalytic degradation of Rhodamine B on tin oxide nanoparticles. Figure 10b show mixed dyes, degradation efficiency of RhB diminished from 86% into 4%, 2%, 33%, 2%, and 47% and efficiency of MGO increased 94–98% to all the trapping agents.

4.2 Mechanism

In general, the preparation of *nano* materials, purity of raw materials, atmosphere, growth rate, and annealing process show a great impact on the type and quantity of defects [39]. On the basis of the above discussion, the different defect types in SnO_2 lead to different band structures. This may have a significant influence on the mechanism for degradation of dye. During the reaction, the molecules are first immobilized on the surface of SnO_2 by chemisorption. The target molecule can then be reduced if the reduction potential matches the conduction band of SnO_2, which depends on the types of defects. If the reduction potential of a dye matched that of the material, a redox reaction would occur and the dye is degraded. Therefore, the reduction property of the dye depends upon the nature of catalyst and surface. A number of factors can affect the efficiency of photodecomposition, such as preparation method, band gap energy and the distribution of the organic molecule on the surface of the particle. The MGO dye shows much higher photodecomposition activity compared with that of RhB. For the *nano* SnO_2 photocatalysts, the degradation increases with catalyst dosage at the optimum concentration, pH and at 254 nm irradiation. The surface affinity of the dye molecule may enhance in the oxidative damage. When the concentration of adsorbed molecule is high, the rate of oxidation is improved because the distance between trapping sites in a particle decreases. It is significant to point out that the photodegradation of MGO

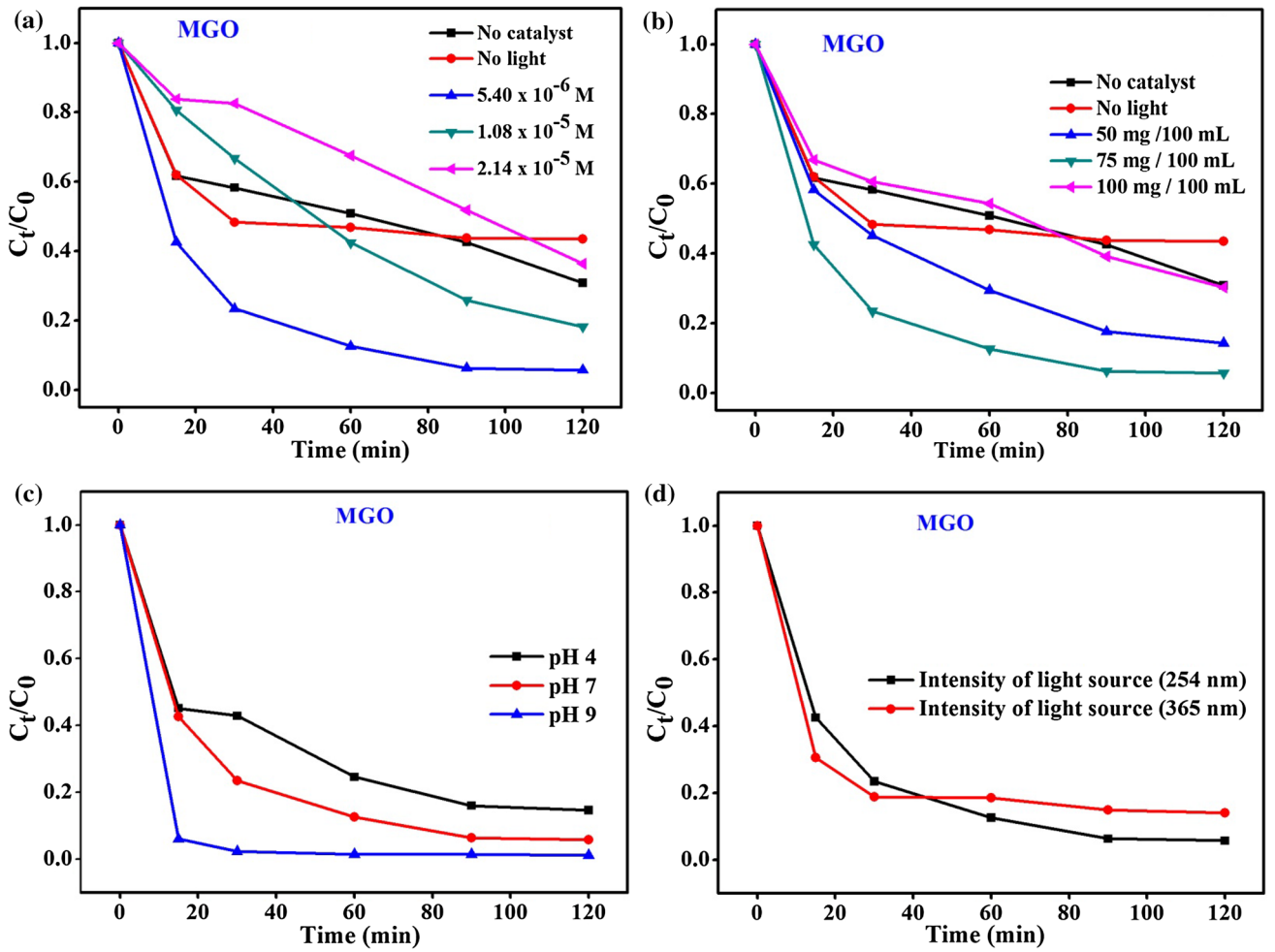

Fig. 9 Factors influencing photocatalytic degradation of malachite green oxalate (λ ~ 616 nm) from the mixtures. Effect of **a** concentration of malachite green oxalate from the mixtures (RhB + MGO), **b** catalyst dosage, **c** pH, **d** intensity of light source (254 and 365 nm)

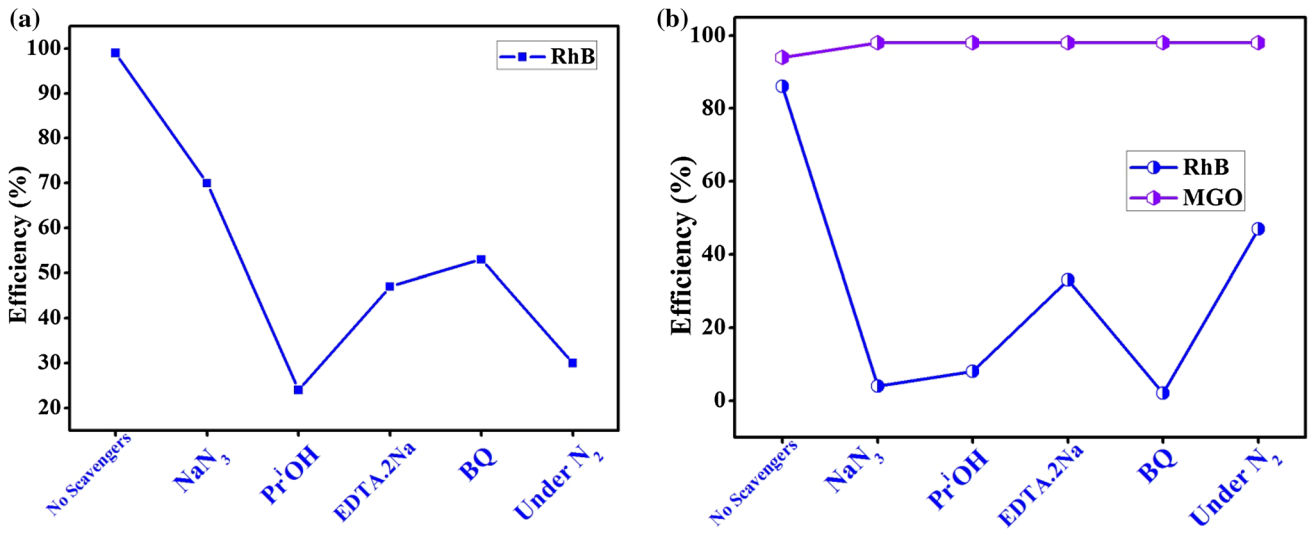

Fig. 10 Degradation efficiency of radical scavenging study on *nano* SnO_2 nanoparticles using Rhodamine B and mixed dye (RhB + MGO) at room temperature

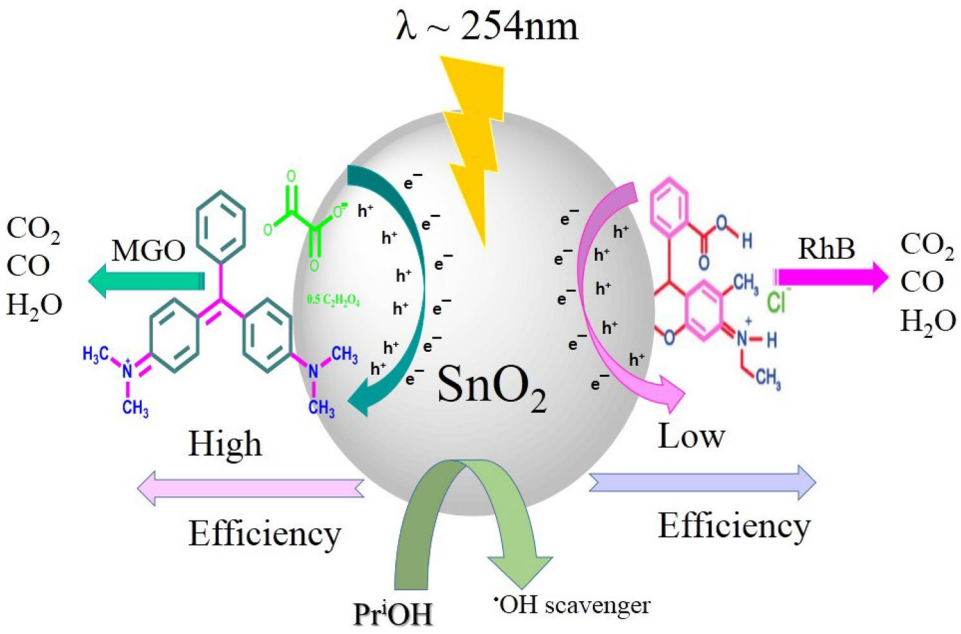

Fig. 11 Degradation pathway of dye molecules

on *nano* SnO_2 is much higher than that of RhB. Figure 11 represents the photocatalytic degradation process of SnO_2 nanoparticles includes chemical steps producing highly reactive species such as hydroxyl radical, superoxides, and hydrogen peroxide, these in principle, can cause fatal damage to organic molecules. In these reactive oxygen species, the hydroxyl radicals are highly reactive and therefore short-lived. The superoxide ions are relatively long lived, but must contact directly the outer surface [40]. Hydrogen peroxide is less harmful compared to hydroxyl radicals and superoxide ions. However, oxygen species contribution to the oxidative reactions with organic compounds is still not very clear. Molecules adsorb on SnO_2 surfaces via (1) molecular, (2) dissociative adsorption processes and (3) monolayer formation. In the molecular adsorption oxygen binds to Sn atom, and the OH group forms a hydrogen bond with a surface oxygen atom. There are several possibilities for dissociative adsorption and one such involves the deprotonation of OH group and the attachment of the H^+ to surface oxygen. The remaining oxygen binds to a surface tin atom producing a monodentate structure. The fact that Sn–O distances for the dissociative modes are shorter than for the molecular adsorption indicates a stronger interaction for the former ones [41].

There are additional inactivation pathways that deserve consideration. Tin oxide has a thermodynamic capacity for this action, with an oxidation potential at its conduction band. For a significant amount of direct oxidation of Rhodamine B and malachite green oxalate to have occurred, the molecule would have to outcompete with oxidative species for oxidation. This adsorption probably resulted from a non-attractive partitioning of the Rhodamine B and malachite green oxalate onto the semiconductor that was ascribable to exclusion of the hydrophobic portions. The greatest damage was most likely caused by •OH radical. Enhanced malachite green oxalate destruction might also be explained by efficient targeting by •OH radical directed by adsorbed sites.

4.3 Catalyst Reusability Test

In photocatalytic reaction, the chemical stability, reusability and recovery is much more important in photocatalytic applications. In this work, catalytic activity experiments were repeated to find out stability of catalyst towards degradation efficiency of Rhodamine B and mixed dye molecules (MGO + RhB) under ultraviolet illumination. SnO_2 exhibited higher ultra-violet active and degradation efficiency of Rhodamine B (99%) and mixed dye molecules (MGO + RhB) up to three cycles as shown in Fig. 12a, b. After completion of three cycles, the catalyst was washed with distilled water several times and dried at 100 °C. The chemical stability of catalyst was confirmed by XRD pattern after completion activity cycles, the peak intensity and positions was unchanged as that of a fresh catalyst. The crystallite size of the freshly prepared and recovered catalyst from RhB, mixed dye molecules (MGO + RhB), slightly increases which was observed after dye degradation (Table 5). From this result the SnO_2 nanoparticles was stable and recyclable even after three cycles towards mixed dye removal of organic pollutants under ultraviolet irradiation. The catalyst can easily be recovered by filtration and can be reused several times without any significant loss of catalytic activity. The catalytic reaction was carried out in the absence of any added base so there is no corrosion problem involved in the process. The

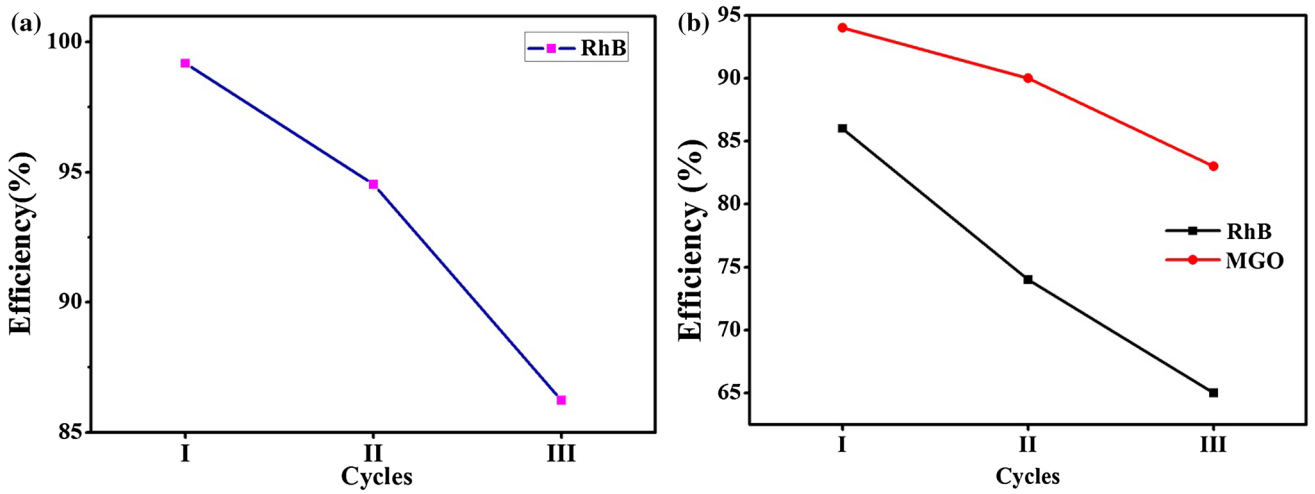

Fig. 12 Reusability of SnO_2 nanoparticles. **a** Efficiency of degradation of Rhodamine B obtained after three cycles. **b** Efficiency of degradation of mixed dye (MGO + RhB) obtained after three cycles

Table 5 XRD pattern of pure tin oxide nanoparticles by simple co-precipitation technique and recovered from after photolysis from Rhodamine B at room temperature

Sample name	Position of (101) peak	FWHM at (101) peak	Vol. of the nanoparticles, V (nm^3)	Lattice parameters			Average crystallite size (nm)[a]
				a (Å)	b (Å)	Unit cell volume $(Å)^3$	
SnO_2 NPs	33.95	0.3360	2691.32	4.7373	4.7373	71.51	15.68
Recovered SnO_2 NPs[a]	33.95	0.3840	5353.62	4.7358	4.7358	71.43	19.72

a = calculated by the scherrer equation from XRD measurements

[a]Recovered from degradation of RhB

reactants were converted into their respective product with a high yield and 100% selectivity in a short time duration, which demonstrates that the surface of the catalyst is highly active.

It is interesting to speculate the role nanoparticles photocatalysis investigation may provide a new platform for new level of chemical engineering applications of the materials. The critical issues for consideration are; (a) better controllability of synthesis, via solution routes; (b) newer and greener chemical synthetic routes should be devised, through water medium and at low temperature, since a number of processes use toxic organic solvents; and (c) scale up methodologies and techniques for large-scale production. Therefore, the present accomplishments, can investigate in greater depths on the nanoscale chemical engineering.

5 Conclusion

In summary, tin oxide nanoparticles were prepared by a simple facile co-precipitation method and exhibited much superior degradation behavior towards degradation of single organic dye. Photocatalytic activities of the samples were examined by employing the photocatalytic degradation of RhB and (RhB + MGO) in water and degradation under ultraviolet irradiation. The effect of dye concentration, quantity of catalyst, pH, and intensity of light source were optimum and investigated in detail. Both the single and mixed dye degradation matched well with pseudo first-order kinetics reactions. Kinetic analysis revealed that the rate controlling steps were the surface reaction of the adsorbed dye molecule for degradation. On comparing photodegradation efficiency, the importance of reactive species in the reaction using different radical scavengers were studied and reusability of the catalyst also performed up to three cycles and stable photocatalysts in the ultraviolet irradiation to degrade multiple contaminant treatment.

Acknowledgements KA records his sincere thanks to the Council of Scientific and Industrial Research-HRDG (EMR Division, No. 01(2953)/18/EMR-II/1.5.2018), New Delhi, for financial support through major research project. The authors thank CIF, Pondicherry University for providing instrumental facility.

References

1. N. Daneshvar, D. Salari, A.R. Khataee, J. Photochem. Photobiol. A **157**, 111 (2003)
2. N. Wetchakun, P. Wanwaen, S. Phanichphant, K. Wetchakun, RSC Adv. **7**, 13911 (2017)
3. H.Y. Li, Y.H. Gong, Q.Q. Huang, H. Zhang, Ind. Eng. Chem. Res. **52**, 15560 (2013)
4. S.G. Seong, E.J. Kim, Y. Kim, K. Lee, S. Hahn, Appl. Surf. Sci. **256**, 1 (2009)
5. J. Sun, X. Li, Y. Quan, Y. Yin, S. Zheng, Chemosphere **136**, 181 (2015)
6. A. Dey, Mater. Sci. Eng. B **229**, 206 (2018)
7. X. Zhou, K. Jia, X. He, S. Wei, P. Wang, X. Liu, Mater. Chem. Phys. **207**, 212 (2018)
8. J. Liqiang, S. Xiaojun, S. Jing, C. Weimin, X. Zili, D. Yaoguo, F. Honggang, Sol. Energy Mater. Sol. Cells **79**, 133 (2003)
9. Q. Wali, A. Fakharuddin, R. Jose, J. Power Sources **293**, 1039 (2015)
10. S. Wang, J. Yang, H. Zhang, Y. Wang, X. Gao, L. Wang, Z. Zhu, Sens. Actuators B **207**, 83 (2015)
11. M. Zhang, Y. Zhen, F. Sun, C. Xu, Mater. Sci. Eng. B **209**, 37 (2016)
12. M.S. Fu, L. Ni, N. Du, J. Alloys Compds. **591**, 65 (2014)
13. Y. Deng, C. Fang, G. Chen, J. Power Sources **304**, 81 (2016)
14. E. Haritha, S.M. Roopan, G. Madhavi, G. Elango, N.A. Al-Dhabi, M.V. Arasu, J. Photochem. Photobiol. B **162**, 441 (2016)
15. D. Zhao, X. Wu, Mater. Lett. **210**, 354 (2018)
16. V.K. Gupta, R. Saravanan, S. Agarwal, F. Gracia, M.M. Khan, J. Qin, R.V. Mangalaraja, J. Mol. Liq. **232**, 423 (2017)
17. A.S. Ganeshraja, K. Rajkumar, K. Zhu, X. Li, S. Thirumurugan, W. Xu, J. Zhang, M. Yang, K. Anbalagan, J. Wang, RSC Adv. **6**, 72791 (2016)
18. P. Zhang, L. Wang, X. Zhang, C. Shao, J. Hu, G. Shao, Appl. Catal. B **167**, 193 (2015)
19. S. Ahmed, M. Rasul, W.N. Martens, R. Brown, M. Hashib, Water Air Soil Pollut. **215**, 3 (2011)
20. A.M. Al-Hamdi, M. Sillanpää, J. Dutta, Res. Chem. Intermed. **42**, 3055 (2016)
21. R. Jain, M. Mathur, S. Sikarwar, A. Mittal, J. Environ. Manag. **85**, 956 (2007)
22. D. Venkatesh, S. Pavalamalar, K. Anbalagan, J. Mater. Sci. Mater. Electron. (Submitted)
23. S. Begum, M. Ahmaruzzaman, Appl. Surf. Sci. **449**, 780 (2018)
24. A.C. Pradhan, M.K. Sahoo, S. Bellamkonda, K.M. Parida, G.R. Rao, RSC Adv. **6**, 94263 (2016)
25. H. Fu, C. Pan, L. Zhang, Y. Zhu, Mater. Res. Bull. **42**, 696 (2007)
26. R. Chen, G.Z. Xing, J. Gao, Z. Zhang, T. Wu, H.D. Sun, Appl. Phys. Lett. **95**, 061908 (2009)
27. K. Suematsu, N. Ma, M. Yuasa, T. Kida, K. Shimanoe, RSC Adv. **5**, 86347 (2015)
28. Y. Chen, B. Qu, L. Hu, Z. Xu, Q. Li, T. Wang, Nanoscale **5**, 9812 (2013)
29. S. Obregón, G. Colón, J. Mol. Catal. A **376**, 40 (2013)
30. A.K. Sinha, M. Pradhan, S. Sarkar, T. Pal, Environ. Sci. Technol. **47**, 2339 (2013)
31. S. Wang, S. Zhou, Appl. Surf. Sci. **256**, 6191 (2010)
32. M.A. Sh. Sohrabnezhad, M. Zanjanchi, Razavi, Spectrochim. Acta A **130**, 129 (2014)
33. M. Wang, J. Han, P. Guo, M. Sun, Y. Zhang, Z. Tong, M. You, C. Lv, J. Phys. Chem. Solids **113**, 86 (2018)
34. I. Poulios, A. Avranas, E. Rekliti, A. Zouboulis, J. Chem. Technol. Biotechnol. **75**, 205 (2000)
35. Q. Yang, F. Chen, X. Li, D. Wang, Y. Zhong, G. Zeng, RSC Adv. **6**, 60291 (2016)
36. W.Q. Cui, H. Wang, Y.H. Liang, Chem. Eng. J. **230**, 10 (2013)
37. L.S. Zhang, K.H. Wong, Z.G. Chen, J.C. Yu, J.C. Zhao, Appl. Catal. A **363**, 221 (2009)
38. F. Li, Z. Li, M. Zhang, Y. Shen, Y. Cai, Y. Li, X. He, C. Chen, RSC Adv. **7**, 34705 (2017)
39. S. Lingyue Liu, G. Shu, Zhang, S. Liu, ACS Appl. Nano Mater. **1**, 31 (2018)
40. G. Fu, P.S. Vary, C.-T. Lin, J. Phys. Chem. B **109**, 18 (2005)
41. P.C. Redfern, P. Zapol, L.A. Curtiss, T. Rajh, M.C. Thurnauer, J. Phys. Chem. B **107**, 11419 (2003)

Publisher's Note Springer Nature remains neutral with regard to jurisdictional claims in published maps and institutional affiliations.